

Article

Techno-Economic Evaluation of Future Thermionic Generators for Small-Scale Concentrated Solar Power Systems

Alessandro Bellucci ^{1,*}, Gianluca Caposciutti ², Marco Antonelli ² and Daniele Maria Trucchi ¹

¹ Istituto di Struttura della Materia (ISM)—Sez. Montelibretti, DiaTHEMA Laboratory, Consiglio Nazionale delle Ricerche, Via Salaria km 29.300, 00015 Monterotondo, Italy

² Dipartimento di Ingegneria dell'Energia, dei Sistemi, del Territorio e delle Costruzioni (D.E.S.Te.C.), Università di Pisa, Largo Lucio Lazzarino snc, 56122 Pisa, Italy

* Correspondence: alessandro.bellucci@ism.cnr.it

Abstract: Small-size concentrated solar power (CSP) plants are presently not diffused due to a too-high levelized cost of electricity (LCoE), contrarily to CSP plants with capacity >100 MW, which provide LCoE < 20 cEUR/kWh. The integration of solid-state converters within CSP plants can enhance the scalability and economic competitiveness of the whole technology, especially at smaller scales, since the conversion efficiency of solid-state converters weakly depends on the size. Here a system with a high-temperature thermionic energy converter (TEC), together with an optical concentrator designed to be cheap even providing high concentration ratios, is proposed to improve the cost-effectiveness of CSP plants, thus achieving conditions for economic sustainability and market competitiveness. This is possible since TEC can act as a conversion topping cycle, directly producing electricity with a possible conversion efficiency of 24.8% estimated by applying realistic conditions and providing useful thermal flows to a secondary thermal stage. Under established technical specifications for the development of optical concentrator and TEC and according to reasonable economic assumptions, the overall plant conversion efficiency is estimated to be 35.5%, with LCoE of 6.9 cEUR/kW and considering the possibility of an 8 h storage tank for a 1 MW input solar energy system. The calculated projected value is an extremely competitive value compared with other available renewable energy technologies at small capacity scales and opens the path for accelerating the deployment of technological efforts to demonstrate the proposed solution.

Keywords: thermionic energy conversion; concentrated solar power; levelized cost of electricity; thermoelectric generation; energy storage



Citation: Bellucci, A.; Caposciutti, G.; Antonelli, M.; Trucchi, D.M. Techno-Economic Evaluation of Future Thermionic Generators for Small-Scale Concentrated Solar Power Systems. *Energies* **2023**, *16*, 1190. <https://doi.org/10.3390/en16031190>

Academic Editors: Maurizio De Lucia, Giacomo Pierucci, Francesco Taddei, Giuseppe Franchini and Giovanni Brumana

Received: 14 December 2022

Revised: 5 January 2023

Accepted: 18 January 2023

Published: 21 January 2023



Copyright: © 2023 by the authors. Licensee MDPI, Basel, Switzerland. This article is an open access article distributed under the terms and conditions of the Creative Commons Attribution (CC BY) license (<https://creativecommons.org/licenses/by/4.0/>).

1. Introduction

The use of efficient, robust, and sustainable solid-state technologies for the conversion of concentrated solar radiation represents the most promising but challenging solution for renewing the interest in the concentrated solar power (CSP) market [1]. Presently, CSP plants are economically sustainable only at large scales (>100 MW), producing electricity with the involvement of heat transfer fluids (HTF) to feed thermal engines, which have high costs of deployment and continuous maintenance. Indeed, the thermal losses accumulating along all the plant components before reaching the downstream thermodynamic engines affect the overall system solar-to-electrical efficiency down to 20%, despite the high thermal-to-electrical efficiency of the converters (up to 35% for electric power levels >10⁴ kW and for operating temperatures > 500 °C) [2]. On the other hand, concentrated photovoltaics (CPV) have far to go to meet the requirements for practical implementation, due to the high fabrication costs of the converter and the thermal operational constraints, despite the very high conversion efficiency (47.1%) [3]. In such a context, one of the most competitive possibilities to increase the overall efficiency of the plants is the use of solid-state converters [1], which are generally connected to advantages implying conversion efficiency not depending

on the active size, absence of moving parts, and reduced production costs from a minimum usage of the active materials. Among solid-state converters for concentrated solar radiation, thermionic-based energy converters (TECs) are emerging as high-temperature solar converters, operating as conversion topping cycles [4,5]. If the thermionic cathode has the functionality of a selective solar absorber, the TECs can be defined as engineered receivers replacing the solar collectors used in the conventional CSP plants, producing electricity as well as feeding secondary conversion stages, which can be constituted by thermodynamic cycles or, alternatively, by a further solid-state converter such as thermophotovoltaic cell at operating temperatures $> 1000\text{ }^{\circ}\text{C}$ [6–8] or a thermoelectric generator [9,10].

The integration of TECs in CSP plants may allow using high radiation fluxes on reduced area receivers. This solution can lead to the realization of small-scale CSP plants. However, the current optical systems are not suitable for an advantageous implementation of widespread and small-scale installations. In fact, among the different concentrating optics types, which differentiate each other depending on the achievable concentrated radiation power density, only solar towers and parabolic dishes allow reaching temperatures higher than $700\text{ }^{\circ}\text{C}$ for the receiver. Anyway, as the concentration ratio increases, more and more precise tracking is required, and the size of the optical system must increase (e.g., dishes may have a total aperture $> 5\text{ m}$) [11]. As the mirrors' size increases, mechanical stresses due to the system weight and to the wind thrusts (apart from all the other weather agents) significantly increase, making these systems expensive and requiring large free portions of soil for their installation to limit mirrors' mutual shading. Considering such aspects, the linear Fresnel reflector is to be preferred to the other ones, since the mirrors are flat, very narrow in cross-section, and easier and cheaper to build. However, the low concentration resulting from linear Fresnel reflectors does not generally allow a receiver to surpass temperatures $> 300\text{ }^{\circ}\text{C}$ [12] and a novel solution is needed for achieving a relatively high concentration ratio.

Due to these considerations, the conceptual development of a pioneering approach for advanced small-scale CSP plants, based on a two-axes tracking solar concentrator, with simplified design and structure, combined to a TEC, in turn feeding thermal energy for energy storage and/or to a secondary stage of energy conversion, deserves to be investigated. Nowadays, even if the technology is still not mature, it is important to estimate if the proposed solution could be cost-effective and competitive if compared with commercially available renewable technologies. In this work, a preliminary techno-economic assessment is performed for this case study, with the aim to evaluate the advantages, the technological constraints, the future costs at a large-market scale, the performance, and the optimistic LCoE achievable for small scales of plants with input power from 50 kW to 1 MW, useful for the needs from residential buildings to industrial applications.

2. Definition of the System

2.1. Optical Concentrator for Small-Size CSP Applications

The linear Fresnel reflectors make use of the Fresnel lens effect, being constituted by a concentrating mirror with a large aperture and a relatively short focal length. Typically, the reflectors are located at the base of the whole system, remaining very close to the supporting structure. Therefore, they are less subject to actions by the wind and other atmospheric agents and have a lighter structure. Furthermore, only a single actuator is needed for sun tracking. Consequently, also the support structure of the mirrors and the receiver is much lighter, which allows a Fresnel system to be placed even on roofs (industrial and residential) and coverings. However, this linear system does not allow for achieving a relatively high concentration ratio. To increase the temperature on the receiver, the development of a novel Fresnel concentrating optics is necessary, which can cope with the opposite requirements of a relatively high concentration ratio, simplicity, lightness, cost-effectiveness, and low soil occupancy.

For CSP plants with a capacity of up to 1 MW, a Bi-Axial Fresnel (BAF) lens system can be considered able to meet all the requirements. A BAF system is constituted by a two-axes

concentrator consisting of flat or slightly curved mirrors. The concentrator is constituted of an array of pivoting frames (Figure 1), each one carrying a plurality of mirrors. The frames can be simultaneously pivoted by a single actuator by means of a mechanical linkage.



Figure 1. Concept of the BAF concentrator.

The similarity of this concept with the conventional Fresnel system is straightforward. In this case, however, the mirrors can be rotated along an axis perpendicular to the axis of the frames. A bi-axial movement is then achieved, with a much-reduced number of servo motors with respect to a conventional bi-axial concentrator, which usually requires two motors per mirror. The precision of the scheme is obviously lower than a full bi-axial system, but its lower cost makes this kind of concentrating optics more suited to small-scale systems. A secondary concentrator can be accommodated in the assembly to both partly compensate for the optical inaccuracies and to further increase the concentration. The concentration ratio is roughly the square of a conventional single-axis Fresnel, thereby allowing a higher operating temperature than traditional Fresnel systems. A much smaller receiver is needed and the cost of the target supporting structure can be reduced as well. An example of the solar concentrator/secondary mirror/receiver is depicted in Figure 2.

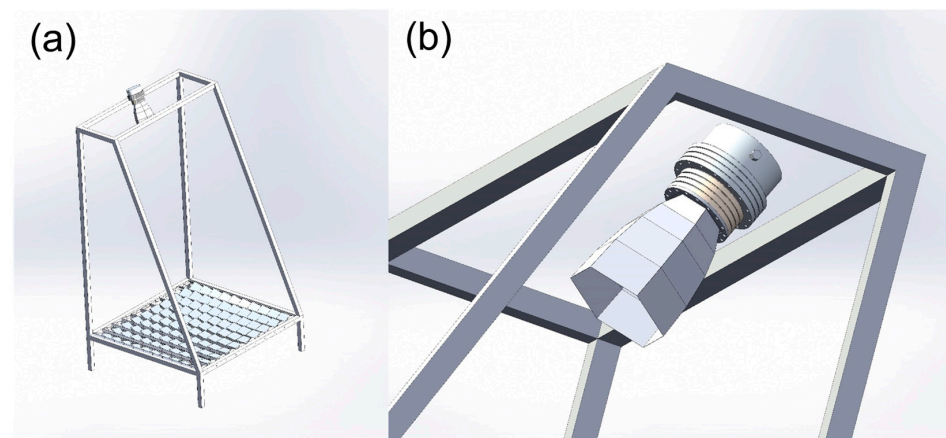


Figure 2. Renderings of: (a) the assembly of the BAF concentrator and the converter; (b) the detail of the receiver equipped with the secondary concentrator mirror system.

The design of practical BAF concentrating optics has been defined by establishing the basic parameters reported in Table 1. With the aim to be conservative in the estimation of the costs and the overall performance, a value of 0.6 for the optical efficiency is considered, that is a value condensing the optical losses of primary and secondary mirrors. The reflective area of the single mirror is fixed to $1.05 \times 1.05 \text{ m}^2$, defined to be the maximum size preserving from problems of structure mechanical stability in the case of extremely harsh weather conditions.

Table 1. Parameters established for the design of BAF concentrating optics.

| Parameter | Value |
|---|-----------------|
| Incident sun power (kW/m ²) | 1 |
| Angle of incidence (average) (deg) | 20 |
| Optical efficiency (%) | 60 |
| Total surface of the single mirror (m ²) | 1.11 |
| Lateral size of the single mirror (m) | 1.05 |
| Materials for the supporting system | Stainless steel |
| Distance between 2 consecutive mirrors (horizontal) (m) | 0.21 |
| Distance between 2 consecutive mirrors (vertical) (m) | 0.79 |

Based on these assumptions, the number of BAF mirrors can be sized according to the input power capacity (from 50 kW to 1 MW) by fixing a constant input power density on the receiver ($P_{in} = 902 \text{ kW/m}^2$). To accomplish such a technological challenge, the secondary mirror is characterized by a decreasing concentration ratio as a function of the plant size, reaching a maximum value of 20 suns. The number of servo motors actuating the sun-tracker depends on the number of necessary mirrors' rows. The receiver is modeled to have a circular shape, the diameter of which is limited to values $\ll 1.5 \text{ m}$, considered as the maximum value to obtain a homogenous surface radiation distribution with the employed optics.

Table 2 reports all the main features of the system according to the 5 different sizes of the CSP plant. The total cost of the system, expressed in EUR/kW (i.e., cost of power) or in EUR/m² (allowing to establish the soil occupation at a given plant capacity), has been calculated considering the commercially available materials' costs. An overhead of 35% on the operating costs has been applied to the total direct costs for contemplating possible extra charges in the processing costs. Even if a direct comparison with CSP cannot be made since CSP plants at small scales are not fully investigated, the estimated costs (details are in Appendix A) are lower than 120–280 EUR/m² which is the range reported for plants larger than 50 MW of electrical production [13]. Moreover, the materials' costs could be even lower if large-scale production of the system will occur. Finally, it is worth noticing that the soil occupancy is far lower than the more consolidated technologies operating at high receiver temperatures, being 3300 m²/MW for the 1 MW input power capacity plant. The use of parabolic trough collector systems is reported in the order of at least 6100 m²/MW for the solar field area [14], which is about double that of a BAF concentrator system.

Table 2. Description of the main components of the BAF system for different plant sizes.

| BAF System for CSP Plant Size | 50 kW | 100 kW | 250 kW | 500 kW | 1 MW |
|---|---------|---------|--------|--------|--------|
| Number of mirrors | 80 | 160 | 400 | 800 | 1600 |
| Number of servo motors | 11 | 26 | 31 | 41 | 47 |
| Concentration primary field/secondary field | 1600/20 | 1600/10 | 1600/4 | 1600/2 | 1600/1 |
| Mirror total surface (m ²) | 89 | 177 | 443 | 887 | 1774 |
| Receiver area (m ²) | 0.055 | 0.11 | 0.28 | 0.55 | 1.1 |
| Receiver circular diameter (m) | 0.266 | 0.376 | 0.594 | 0.840 | 1.188 |
| Occupied soil (m ²) | 54 | 163 | 511 | 1244 | 3270 |
| Cost/kW (EUR/kW) | 465 | 540 | 436 | 393 | 367 |
| Cost/m ² (EUR/m ²) | 431 | 330 | 213 | 158 | 112 |

A very elementary, lab-scale prototype was developed and built (Figure 3) for the first experimental campaign, which is currently in progress. In the picture, it is possible to observe the concentrated beam impinging the monitoring screen on the top, whereas the movement system with the mirrors is located at the bottom of the prototype.

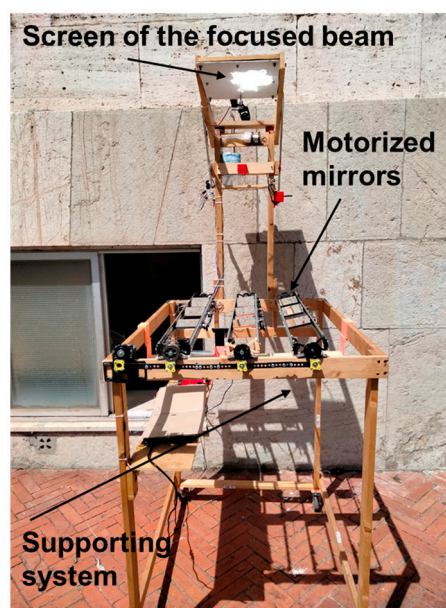


Figure 3. Picture of the first lab-scale prototype under test. Arrows and labels have been added to better identify the main elements of the concentrator.

2.2. TECs as CSP Engineered Receiver

The integration of a TEC in CSP plants can improve the overall conversion efficiency of the whole system, since a TEC receiver can efficiently absorb the concentrated sunlight, similarly to the state-of-the-art receivers, and produce an additional quantity of electricity, notwithstanding it can feed a secondary electrical or thermal stage. This is possible since the architecture of a TEC is constituted by an electrode (cathode) acting as both absorber and electrons' emitter, which operates at a temperature T_C that is much higher than the temperature T_A of the second electrode (anode). Besides establishing the Carnot limit, the difference between T_C and T_A defines the maximum performance of the converter and depends on the thermally conductive and radiative energy fluxes within the converter. Moreover, the two electrodes must be separated by small gaps estimated to be in the range $0.3\text{--}3\ \mu\text{m}$ [15,16] to maximize the TEC conversion efficiency, since small gaps avoid space charge effects limiting the device current and too small gaps induce near-field conditions causing anode overheating. To accomplish it, many strategies were pursued but the use of solid dielectric microspacers (DMS) seems to be the most challenging but practical solution. Recently, the use of zirconia DMS arranged in a specific pattern was demonstrated in practical thermionic-based applications up to $1350\ \text{°C}$ [17]. According to the thermal simulations, a thermal gradient of about $700\ \text{°C}$ when the cathode is impinged by an input radiative flux of $90\ \text{W}/\text{cm}^2$ can be established under optimized conditions.

If the anode, cathode, and absorber have the same active area, the TEC conversion efficiency η_{TEC} can be defined as:

$$\eta_{\text{TEC}} = (J_{\text{TEC}} \cdot V_{\text{OUT}}) / P_{\text{in}}, \quad (1)$$

where J_{TEC} is the net thermionic current density and V_{OUT} is the output voltage, which, under ideal operating conditions, is the difference between the cathode work function (Φ_C) and the anode one (Φ_A) divided by the electron charge q .

J_{TEC} is the difference between the cathode current density and the anode one:

$$J_{\text{TEC}}(V_{\text{OUT}}) = (J_{\text{Ti,C}}(V_{\text{OUT}}) - J_{\text{Ti,A}}(V_{\text{OUT}})), \quad (2)$$

where $J_{\text{Ti,C}}$ and $J_{\text{Ti,A}}$ are the cathode and anode current densities at the voltage V_{OUT} , respectively.

The thermionic saturation current density J_{TI} for the two electrodes is equal to:

$$J_{TI} = A_R \cdot T^2 e^{(-\Phi/(k_B \cdot T))}, \quad (3)$$

where A_R is the Richardson constant, T the temperature, Φ the work function of each electrode, and k_B is the Boltzmann constant.

To evaluate the performance of the TEC as a conversion topping cycle for small-size CSP plants, the analytic model implemented in a previous work [9] is here employed, in order to take into account the thermal fluxes losses (emissive, conductive, ohmic, and thermionic cooling losses) involved in the process. Some realistic assumptions are made: (1) the input solar flux is fixed to 90.2 W/cm^2 ; (2) the cathode and the anode substrates are molybdenum (Mo) and copper (Cu), respectively; (3) thermally and chemically stable thin-films are applied on both the cathode and the anode substrates' inner surface, to form the thermionic emitter and collector, respectively, and suitably engineering the electrodes' work functions; (4) the optical properties of such thin-films are considered not to affect the thermal balance equations in the thermo-radiative contributions; (5) the maximum achievable cathode temperature is $1400 \text{ }^\circ\text{C}$; (6) the maximum achievable temperature difference between the electrodes is $700 \text{ }^\circ\text{C}$; (7) the anode temperature T_A is a free parameter, that corresponds to the case of complete control of heat extraction from the anode; (8) no space charge conditions occur, therefore the device operates under ideal electron transport conditions.

The physical properties used in the model are resumed in Table 3. As in the case of the BAF concentrator design, a conservative approach is applied for the evaluation of the TEC performance by considering a value of A_R for the emitter which is half of the ideal value (contrarily to that of the anode, considered as $120 \text{ A cm}^{-2}\text{K}^{-2}$). As regards the optical properties of the cathode, a constant spectral selectivity α/ε of 2.42 is considered a function of temperature, with a solar absorptance α of 88% and a thermal emittance of 35%. These values can be obtained by applying a surface nanostructuring that enhances the absorber material's optical properties, as already reported for other ceramic absorbers [18,19].

Table 3. Main properties of the materials involved in the evaluation of the TEC performance.

| Materials' Properties for TEC Design | Value |
|---|---------|
| Window transmittance (a.u.) | 0.92 |
| Cathode solar absorptance α (a.u.) | 0.88 |
| Cathode thermal emittance ε (a.u.) | 0.35 |
| Emitter thermal emittance (a.u.) | 0.40 |
| Collector thermal emittance (a.u.) | 0.10 |
| Emitter Richardson constant ($\text{A K}^{-2} \text{ cm}^{-2}$) | 60 |
| Collector Richardson constant ($\text{A K}^{-2} \text{ cm}^{-2}$) | 120 |
| Electrical cables (copper) length (mm) and cross-sectional area (mm^2) | 300, 50 |

Figure 4a shows the values of the TEC conversion efficiency obtained as a function of the emitter work function for different T_A values at fixed anode work function $\Phi_A = 1.2 \text{ eV}$. Figure 4b shows the efficiency obtained as a function of the emitter work function by varying the Φ_A values from 1.0 to 1.4 eV at fixed $T_A = 600 \text{ }^\circ\text{C}$.

The best condition of $\eta = 27.6\%$ is found for $T_A = 600 \text{ }^\circ\text{C}$, $\Phi_A = 1.2 \text{ eV}$, and $\Phi_C = 2.1 \text{ eV}$. Under these conditions, the cathode temperature is equal to $1275.2 \text{ }^\circ\text{C}$ and the $V_{OUT} = 0.9 \text{ V}$. Obviously, the implementation of such materials in a TEC today still represents a materials science challenge. However, barium-based coatings have values very close to the desired ones for both the electrodes' work function, such as barium fluoride [20], barium oxide [21], or barium–strontium composites [22]. Even if these materials should be stable at the expected working temperatures, the thermal properties of the thin films must be deeply investigated during long-term operations.

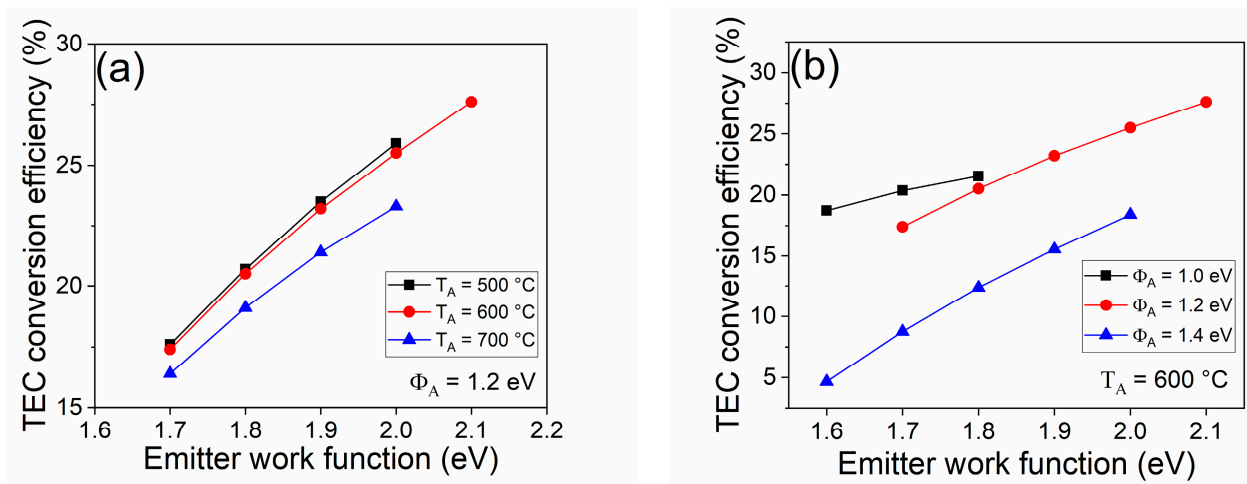


Figure 4. TEC conversion efficiency as a function of the emitter work function considering different conditions for the anode temperature (a) and the anode work function (b). All the values reported in the plots derive from calculations meeting all the constraints declared in the text. In particular, the values for which the cathode temperature results $>1400\text{ }^{\circ}\text{C}$ and the temperature difference between the electrodes $>700\text{ }^{\circ}\text{C}$ are not plotted because considered physically unfeasible.

An important aspect to be considered for the TEC deployment is the maximization of the electrical output. Since the output voltage is too low for providing power to the grid, an electrical system to handle and manage the power output is mandatory. In this framework, one of the possible strategies to be pursued is to consider an arrangement of smaller converters forming the total area TEC receiver, which are connected electrically in series. This modular approach has the advantage of increasing the output voltage of the converter, to decrease the current flowing along the electrical cables, but can be limited by the lowest current provided by a single converter. As for photovoltaics, this is solved by a high reproducibility of the elementary converters and is connected with a high level of industrial maturity of the technology. In the techno-economic analysis, this kind of solution has been provided; however, the use of modular converters and their connection will be a crucial aspect to be optimized in a future exploitation.

2.3. Hybridization of TEC with Secondary Conversion Stages

The advantage connected to the parallel-plate architecture of a TEC is in the matching of a secondary stage of conversion. The thermionic anode collects a thermal flux which can be converted. On the other hand, heat dissipation from the anode is vital to avoid overheating. As shown in the evaluation of the TEC performance, a lower anode temperature improves the conversion efficiency at the given thermionic properties of the electrodes (e.g., for $\Phi_C = 2.0$, $\eta = 25.9\%$ and 25.4% at $T_A = 500\text{ }^{\circ}\text{C}$ and $600\text{ }^{\circ}\text{C}$, respectively). In this study, two different solutions for the secondary stage are analyzed (as shown in Figure 5):

(1) The use of thermoelectric generators (TEG), that can exploit the exhaust heat producing instantaneous electrical power when a temperature difference is established between the two sides of the generator. In this case, TEGs will be mounted directly in contact with the bottom surface of the anode (i.e., the opposite face with respect to the TEC structure). An additional cold plate component and related cost must be considered for the TEG cooling so to maintain a suitable thermal gradient for maximizing the output power.

(2) The use of a thermal storage system, based on heat transfer fluid (HTF) technology (depending on operating temperatures), feeding on demand for example a Stirling engine, which can provide additional electricity when desired. In this case, the presence of a suitable tank is considered for the thermal exchange with the HTF sub-system, whereas conventional blocks for the thermal energy storage and the Stirling engine can be used.

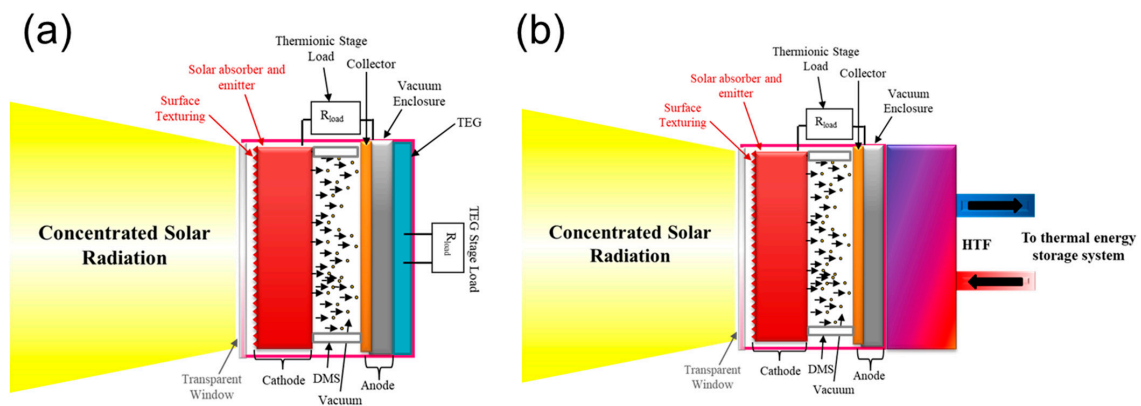


Figure 5. Sketch of the possible hybridization of TEC with (a) TEG modules and (b) HTF sub-system.

3. Economic Evaluation: LCoE Calculation

The proposed solutions for the installation of small-size CSP plants with TEC integration provide several advantages from the economic point of view: (1) the use of thin-film technologies for obtaining the desired functionalities of the thermionic engineered electrodes, which are techniques that can be suitably applied on large areas and large scales at low production costs; (2) the selection of bulk materials (i.e., substrates for the thin-film depositions) with the condition of abundance and wide availability on the market; (3) an innovative optical system for concentrating the solar radiation which is compact, light, easy-to-manage, and cheap.

The purpose of this work is to evaluate in a very preliminary way the costs of such a structure, considering the costs on a large-market scale. Despite the technology is not mature and some assumptions can result in being too speculative, a detailed analysis has been carried out by applying an average of the prices available in the cost catalogs provided by the main producers. In order to use this work as a guide for a future exploitation, a model of costs is detailed in Appendix A with the aim to revise the assessment according to re-actualizations of the costs.

Table 4 shows the main fixed parameters used for the techno-economic analysis. The TEC is designed as a vacuum cylinder with a height of 25 cm in which all the elements are enclosed and provided with electrical and thermal feed-throughs. The use of an electronic stage (i.e., DC-DC converters) is considered for the electrical output power management, with an electrical-to-electrical efficiency fixed to 90% (with a double boost of conversion from low voltages, considering the efficiency of the single stage of 95%), reducing the total TEC conversion efficiency to 24.8%. The thermal-to-thermal efficiency applied to the residual heat is fixed at 65%, considering some heat losses in the coupling between the TEC anode and the cascaded thermal system. The storage capacity was fixed at 8 h, which is an average value with respect to those reported for the present CSP plants. As regards TEG and Stirling thermal-to-electrical efficiencies, the values are cautiously fixed to 5% and 33%, respectively, even if both the efficiencies could potentially be higher [23].

Table 4. Main parameters used for the LCoE calculations.

| Parameters for the Techno-Economic Analysis | Value |
|--|-------|
| Reference direct normal irradiance (DNI) value, annual (kWh) | 1600 |
| TEC efficiency, η_{TEC} (%) | 27.6 |
| TEC height (m) | 0.25 |
| Electrical-to-electrical efficiency (%) | 90.0 |
| Thermal-to-thermal efficiency, η_{TH} (%) | 65.0 |
| TEG efficiency, η_{TH} (%) | 5.0 |
| Stirling efficiency, η_{STI} (%) | 33.0 |
| Storage capacity (h) | 8 |
| Plant lifetime (years) | 25 |

For the evaluation of the LCoE, the costs of TEC materials and manufacturing, TEG, Stirling engines, HTF sub-system, storage energy systems mechanical and electrical parts have been retrieved from different sources, mainly from the website of the main producers. All the applied formulas for the final costs are reported in Appendix A.

Table 5 shows the values of LCoE for CSP plants from 50 kW to 1 MW of input power.

Table 5. Comparison of LCoE for the different options considered with the TEC integration and the use of BAF concentrator for small-size CSP.

| LCoE (EUR/kWh) | 50 kW | 100 kW | 250 kW | 500 kW | 1 MW |
|-----------------------------|-------|--------|--------|--------|-------|
| TEC/Storage/Stirling | 0.085 | 0.078 | 0.073 | 0.072 | 0.069 |
| TEC/TEG (ST ² G) | 0.433 | 0.224 | 0.096 | 0.053 | 0.035 |

If compared with current LCoE estimations for large-scale CSP and utility-scale PV, the value found for a 1 MW plant with a storage system (presenting a total efficiency of 35.5%) is extremely competitive, just in line with the estimated LCoE for PV [24] and even with an optimistic design made for 1 MW electric output power capacity in different sites in Morocco using parabolic trough collectors and commercial power blocks [25]. The reported values accomplish the perspective of LCoE of future plants with the integration of innovative components. [26] Up to 100 kW plant capacity, the estimated LCoE value is between 7.8 and 8.5 cEUR/kWh for the TEC/Storage/Stirling system. Even if higher than PV panels, this value results in being competitive if compared to PV plants equipped with electrical storage systems (i.e., electrochemical batteries) for which the LCoE is presently between 5.21 and 19.72 cEUR/kWh depending on the size of the PV system, the solar irradiation, and the cost of the battery (ranging from 500 to 1200 EUR/kWh) [27].

As regards the hybrid solution with TEG, only at the maximum considered scale it seems to become convenient with respect to PV technology. Since ST²G does not present any storage system, new solutions in terms of materials (e.g., the thermoelectric material SnSe [28]) or thin-film architecture [29,30] must be implemented to be more competitive in the instantaneous power dispatchment market, which is currently ruled by PV.

Figure 6 shows the cost break-ups for the analyzed 50 kW and 1 MW plants. For the small-scale CSP systems, it is possible to state that the BAF optics represents the major costs, which decrease when the size increases. Conversely, TEC increases its costs for larger plants but remains <12%. The low share of costs for the thermal energy storage and HTF subsystems is justified by the reduced quantity of energy to store and dispatch due to the reduced plant capacity. Finally, as described above, the possibilities of significant cost reduction for the solar field may be available, by providing series production and/or more defined designs.

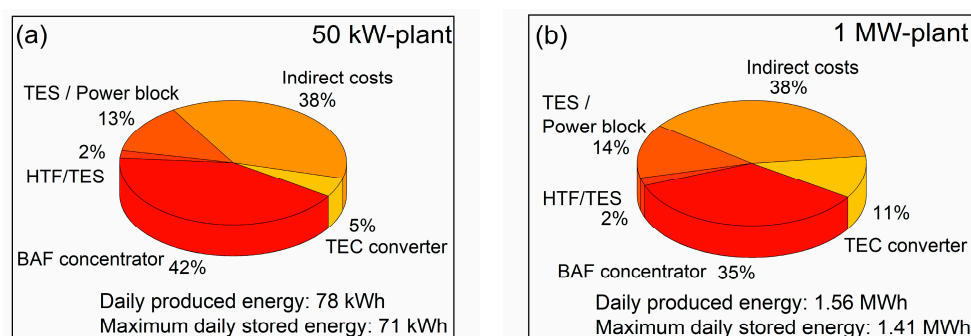


Figure 6. Cost break-up of a 50 kW (a) and 1 MW (b) CSP plant based on a BAF concentrator with TEC integration and 6 h of thermal energy storage. The maximum daily stored energy represents the total available thermal energy if it is not converted by the secondary power block (i.e., Stirling engine). The indirect costs consist mainly of ground rent, integration costs, cost of ownership and maintenance over the considered plant lifetime.

4. Conclusions

The introduction of a thermionic energy conversion stage, together with the use of a bi-axial concentrator system, resulted strongly competitive coupled to an HTF-based storage system for the development of small-scale CSP plants for at least 3 main factors: (1) the total conversion efficiency is 35.5%, much higher than the efficiency of present CSP plants; (2) the soil occupancy is extremely lower than other solar concentrated technology; (3) the expected LCoE is 8.5 cEUR/kWh and 6.9 cEUR/kWh for the 50 kW and 1 MW input power capacity plants at a reference annual DNI of 1600 kWh, getting the technology economically feasible. To accomplish this condition, technical indications have been provided for designing both the concentrator and the properties of the TEC electrodes. Finally, the performed LCoE analysis gives a clear indication that the proposed solution is expected to be advantageous in both the domestic- and utility-scale segments. The very high potential can push the efforts towards technological developments and more sophisticated economic projections to refine in a specialized way all the involved costs.

Author Contributions: Conceptualization, A.B. and D.M.T.; methodology, A.B., G.C., M.A. and D.M.T.; software, A.B.; validation, A.B., M.A. and D.M.T.; formal analysis, A.B.; writing—original draft preparation, A.B.; writing—review and editing, D.M.T.; visualization, A.B. and M.A.; supervision, D.M.T.; funding acquisition, D.M.T. All authors have read and agreed to the published version of the manuscript.

Funding: This research was funded by the European Union’s Horizon 2020 research and innovation program, Future Emerging Technologies (FET) Innovation Launchpad (ILP) action, under the project “TECSAS—Thermionic Energy Conversion & Storage Applied to Sunlight: Taking Concentrating Solar Power to the next level”, Grant Agreement No. 101034922. website: www.tecsas-project.eu; <https://cordis.europa.eu/project/id/101034922>. The accessed dates for the links are 20 January 2022. The sole responsibility for the content of this publication lies with the authors.

Data Availability Statement: Not applicable.

Acknowledgments: The authors thank Stefano Gay of the company Day One for the fruitful discussions.

Conflicts of Interest: The authors declare no conflict of interest.

Appendix A

The economic assessment of the proposed CSP plants has been performed by considering five different contributions to the total costs:

1. Optics (i.e., BAF concentrator),
2. TEC,
3. HTF sub-system and thermal energy storage,
4. Power block (i.e., Stirling engine or TEGs),
5. Indirect costs.

For each of them, the costs were estimated based on an average cost per specific unit, deriving from a market survey of similar items provided by different producers, and under reliable assumptions.

In order to derive the final LCoE, the power produced by the system installed in a medium/high sunny location ($\text{DNI} = 1600 \text{ kWh}/(\text{m}^2 \text{ year})$), which is assumed as a reference DNI annual value, over a lifetime of 25 years, is divided by all the costs of the technology.

In the following, the calculations at the basis of the economic model are reported for each contribution:

Appendix A.1 Optics

The parameters used for the evaluation of the BAF concentrator as a function of the different plant sizes are reported in Tables 1 and 2 of the main text. The estimation of the costs of each sub-component is resumed in Table A1.

Table A1. List of the estimated costs for each sub-component of the optical system. UPN refers to the European standard U.

| Component | Cost |
|--|-----------------------|
| Section bars for the supporting system (UPN $40 \times 20 \times 4 \text{ cm}^3$) | 60 EUR/m |
| Section bars for the mirrors' frames (UPN $20 \times 10 \times 3 \text{ cm}^3$) | 20 EUR/m |
| Mirrors | 10 EUR/m ² |
| Bearing | 5 EUR/unit |
| Servo motor | 250 EUR/unit |
| Sensors | 100 EUR/unit |
| Controllers | 70 EUR/unit |

The total cost of the concentrator optics is the sum of the costs of the three main components, with the addition of manufacturing overhead costs equal to 35% of the total direct costs to consider extra-charges. The total direct costs related to the three main components are: (1) supporting structure (Cost_{ss} , that is equal to the product of the total length of the section bars to the cost per m), (2) mirrors plus frames ($\text{Cost}_{\text{m\&f}}$, that is equal to the sum of three goods: total length of the section bars to the cost per m + total number of bearings to the cost per unit + total mirror surface to the cost per m²), and (3) servo motors plus controls ($\text{Cost}_{\text{servo}}$, that is the sum of three goods: total number of servo motors to the cost per unit + total number of sensors to the cost per unit + total number of controllers to the cost per unit). Table A2 reports the details of the sub-components for the different sizes of CSP plants, used for the calculated estimations.

Table A2. Description of the elements for the optical system as a function of the size (in terms of input power) of the CSP plant.

| Sub-Components | 50 kW | 100 kW | 250 kW | 500 kW | 1 MW |
|--|-------|--------|--------|--------|--------|
| Number of bearings (unit) | 210 | 370 | 860 | 1680 | 3292 |
| Number of sensors (unit) | 4 | 12 | 28 | 53 | 105 |
| Number of controllers (unit) | 11 | 26 | 31 | 41 | 47 |
| Total length of section bars for the mirrors' frames (m) | 210.3 | 609.7 | 1407.2 | 2652.6 | 5259.7 |
| Total length of section bars for the supporting system (m) | 32.6 | 53.9 | 95.0 | 148.7 | 240.2 |

Appendix A.2 TEC Converter

Table A3 shows the estimation of the costs for all the components and processes needed for the TEC fabrication. The TEC receiver consists of a disc-shaped Mo cathode, surface textured by fs-laser on the surface receiving the solar radiation [31] and hosting a thermionic emitter coating on the other surface, of a copper anode covered by a dedicated thermionic collector coating, and of DMS made of dielectric materials. A stainless steel vacuum enclosure with a quartz window allowing cathode illumination and vacuum sealing materials complete the necessary components for a TEC. The total cost depends on the receiver area (which is a function of the CSP plant size).

As regards the costs related to the different technological processes (excluding the direct costs of the material, i.e., Mo and Cu substrates and quartz window), each cost has been estimated by considering the investment in the equipment apparatus (e.g., laser setup, sputtering systems, etc.), depreciated over a standard lifetime of 5 years, and the contribution of consumables, payment of technicians (fixed to 120 kEUR/year) and supply of electrical energy (which depends on the specific technological process), according to the Table A4.

Table A3. List of the estimated prices for each sub-component of the TEC.

| Component | Cost (EUR/cm ²) |
|--|-----------------------------|
| Mo absorber substrate (thickness = 1 mm) | 0.192 |
| Surface laser texturing of the absorber | 0.011 |
| DMS | 0.044 |
| Emitter coating | 0.012 |
| Cu anode substrate (thickness = 1 mm) | 0.036 |
| Collector coating | 0.07 |
| TEC vacuum enclosure | 0.4 |
| Quartz window | 0.003 |
| Vacuum sealing | 0.310 |
| Extra manufacturing costs (for modular converters) | 0.092 |

Table A4. Estimation of the cost in EUR/cm² for the different technologies involved in the TEC fabrication.

| | Surface Texturing | Emitter Coating | DMS | Collector Coating |
|---|--------------------------------------|--|--|--|
| Equipment investment (depreciated) | 60 kEUR/year | 40 kEUR/year | 40 kEUR/year | 40 kEUR/year |
| Technicians | 120 kEUR/year | 120 kEUR/year | 120 kEUR/year | 120 kEUR/year |
| Consumables | 30 kEUR/year | 100 kEUR/year | 40 kEUR/year | 100 kEUR/year |
| Maintenance | 7 kEUR/year | 10 kEUR/year | 10 kEUR/year | 10 kEUR/year |
| Yield | 3600 cm ² /h | 4300 cm ² /h | 900 cm ² /h | 450 cm ² /h |
| Annual production (h ₂₄ /220 days) | 19 × 10 ⁶ cm ² | 23.1 × 10 ⁶ cm ² | 4.75 × 10 ⁶ cm ² | 2.37 × 10 ⁶ cm ² |
| Cost (EUR/cm ²) | 0.011 | 0.012 | 0.044 | 0.07 |

In addition to these costs, the pumping system must be included in the cost of the converter. This cost has been extrapolated by considering the rotary and turbomolecular pumping speed as a function of the converter volume (vol) to be pumped, the production costs of the pump and fixing a factor which involves the operating pressure and the relationship between volume and pressure. Finally, the dependence of the cost is a function of the pumped volume through the phenomenological equation: $Cost_{pumping} = 924 \times e^{0.0015 \cdot vol}$ (EUR).

Finally, the costs related to the electrical output power management must be included. Considering that a real evaluation is rather difficult at this stage, the total cost has been overestimated and fixed to 60% of the total direct costs assumed for the TEC fabrication.

Table A5 reports the total costs for the TEC as a function of the CSP plant size.

Table A5. Calculation of the costs for the complete TEC system production.

| Costs (EUR) | 50 kW | 100 kW | 250 kW | 500 kW | 1 MW |
|------------------------------------|-------|--------|--------|--------|--------|
| Vacuum encapsulated TEC | 1779 | 2700 | 5852 | 13860 | 72338 |
| Electrical power management system | 1067 | 1620 | 3511 | 8316 | 43403 |
| Total cost | 2847 | 4320 | 9363 | 22176 | 115741 |

Appendix A.3 HTF Sub-System and Thermal Energy Storage

The estimated total cost of this component depends on the thermal power to be managed and stored (P_{stored}) which flows from the TEC anode: $P_{stored} = C \times P_{in} \times (1 - \eta_{TEC}) \times \eta_{TH}$, being $C = 0.66$ the loss factor considering the storage plant capacity (8 h), and then assuming a thermal loss of 44% for the storage system with respect to the potential 12 h of continuous irradiance, and P_{in} the capacity input power of the plant. Regarding the use of TEGs, the thermal power P_{th} is directly converted without storage. Table A6 resumes the P_{stored} for the different sizes of the CSP plant.

Table A6. Calculation of the P_{stored} as a function of the CSP plant size, together with the converted power by the Stirling engine and the TEG sub-system.

| Power | 50 kW | 100 kW | 250 kW | 500 kW | 1 MW |
|---|-------|--------|--------|--------|------|
| P_{stored} (kW) | 16 | 32 | 81 | 161 | 322 |
| Converted power by Stirling engine (kW) | 5.3 | 10.6 | 26.6 | 53.2 | 106 |
| P_{th} (kW) | 24 | 49 | 122 | 244 | 489 |
| Converted power by TEGs (kW_e) | 1.2 | 2.4 | 5.9 | 11.8 | 24 |

Based on the considered reference DNI, the total cost is 48 EUR/kWh, where 7.3 EUR/kWh is the cost of the HTFs (734 EUR/m³ as materials costs and 100 kWh/m³ as sizing factor) and 40.7 EUR/kWh is the total cost of the tanks (sized with respect to the chosen capacity), the insulation materials, and the pipes.

Appendix A.4 Power Block

For this sub-component, the cost of the Stirling engine and TEG is fixed at 3.6 kEUR/kW and 0.9 EUR/cm², respectively. For the calculation of the total costs, the power available for the Stirling cycle is equal to the P_{stored} divided by the storage capacity (8 h), whereas the total TEG area is the same as the TEC receiver, considering the same dimensions for both the TEC electrodes.

Appendix A.5 Indirect Costs

As declared in the main text, the indirect costs include ground rent, integration costs, cost of ownership and maintenance of the plant. These costs are estimated as the product of a defined percentage M (2.5% and 1.5% for the TEC/Storage/Stirling and TEC/TEG systems, respectively) of the total direct costs ($\text{Cost}_{\text{direct}}$) to the lifetime of the plant (i.e., 38% of the total direct costs) [32]: $\text{Cost}_{\text{indirect}} = M \times \text{Cost}_{\text{direct}} \times 25$.

References

- Henry, A.; Prasher, R. The prospect of high temperature solid state energy conversion to reduce the cost of concentrated solar power. *Energy Environ. Sci.* **2014**, *7*, 1819–1828. [CrossRef]
- Vining, C.B. An inconvenient truth about thermoelectrics. *Nat. Mater.* **2009**, *8*, 83–85. [CrossRef] [PubMed]
- Geisz, J.F.; France, R.M.; Schulte, K.L.; Steiner, M.A.; Norman, A.G.; Guthrey, H.L.; Young, M.R.; Song, T.; Moriarty, T. Six-junction III–V solar cells with 47.1% conversion efficiency under 143 Suns concentration. *Nat. Energy* **2020**, *5*, 326–335. [CrossRef]
- Bellucci, A.; Girolami, M.; Mastellone, M.; Orlando, S.; Polini, R.; Santagata, A.; Serpente, V.; Valentini, V.; Trucchi, D.M. Novel concepts and nanostructured materials for thermionic-based solar and thermal energy converters. *Nanotechnology* **2020**, *32*, 024002. [CrossRef] [PubMed]
- Campbell, M.F.; Celenza, T.J.; Schmitt, F.; Schwede, J.W.; Bargatin, I. Progress Toward High Power Output in Thermionic Energy Converters. *Adv. Sci.* **2021**, *8*, 2003812. [CrossRef]
- Qiu, H.; Lin, S.; Xu, H.; Hao, G.; Xiao, G. Experimental and theoretical study on hybrid thermionic-photovoltaic energy converters with graphene/semiconductor Schottky junction. *Energy Convers. Manag.* **2023**, *276*, 116584. [CrossRef]
- Bellucci, A.; García-Linares, P.; Martí, A.; Trucchi, D.M.; Datas, A. A Three-Terminal Hybrid Thermionic-Photovoltaic Energy Converter. *Adv. Energy Mater.* **2022**, *12*, 2200357. [CrossRef]
- Bellucci, A.; Mastellone, M.; Serpente, V.; Girolami, M.; Kaciulis, S.; Mezzi, A.; Trucchi, D.M.; Antolin, E.; Villa, J.; García-Linares, P.; et al. Photovoltaic Anodes for Enhanced Thermionic Energy Conversion. *ACS Energy Lett.* **2020**, *5*, 1364–1370. [CrossRef]
- Trucchi, D.M.; Bellucci, A.; Girolami, M.; Calvani, P.; Cappelli, E.; Orlando, S.; Polini, R.; Silvestroni, L.; Sciti, D.; Kribus, A. Solar Thermionic-Thermoelectric Generator (ST2G): Concept, Materials Engineering, and Prototype Demonstration. *Adv. Energy Mater.* **2018**, *8*, 1802310. [CrossRef]
- Bellucci, A.; Mastellone, M.; Girolami, M.; Serpente, V.; Trucchi, D.M. Novel concepts and nanostructured materials for thermionic-based solar and thermal energy converters. *Sol. Energy Mater. Sol. Cells* **2021**, *223*, 110982. [CrossRef]
- Kribus, A. Concentrating solar thermal power. In *Fundamentals of Materials for Energy and Environmental Sustainability*; Ginley, D.S., Cahen, D., Eds.; Cambridge University Press: New York, NY, USA, 2012; pp. 272–288.
- Barlev, D.; Vidu, R.; Stroeve, P. Innovation in concentrated solar power. *Sol. Energy Mater. Sol. Cells* **2011**, *95*, 2703–2725. [CrossRef]

13. Aseri, T.K.; Sharma, C.; Kandpal, T.C. Estimation of capital costs and techno-economic appraisal of parabolic trough solar collector and solar power tower based CSP plants in India for different condenser cooling options. *Renew. Energy* **2021**, *178*, 344–362. [[CrossRef](#)]
14. Aseri, T.K.; Sharma, C.; Kandpal, T.C. Cost reduction potential in parabolic trough collector based CSP plants: A case study for India. *Renew. Sustain. Energy Rev.* **2020**, *138*, 110658. [[CrossRef](#)]
15. Lee, J.-H.; Bargatin, I.; Melosh, N.A.; Howe, R.T. Optimal emitter-collector gap for thermionic energy converters. *Appl. Phys. Lett.* **2012**, *100*, 173904. [[CrossRef](#)]
16. Rahman, E.; Nojeh, A. Interplay between Near-Field Radiative Coupling and Space-Charge Effects in a Microgap Thermionic Energy Converter under Fixed Heat Input. *Phys. Rev. Appl.* **2020**, *14*, 024082. [[CrossRef](#)]
17. Bellucci, A.; Sabbatella, G.; Girolami, M.; Mastellone, M.; Serpente, V.; Mezzi, A.; Kaciulis, S.; Paci, B.; Generosi, A.; Polini, R.; et al. Dielectric Micro- and Sub-Micrometric Spacers for High-Temperature Energy Converters. *Energy Technol.* **2021**, *9*, 200078. [[CrossRef](#)]
18. Sani, E.; Sciti, D.; Silvestroni, L.; Bellucci, A.; Orlando, S.; Trucchi, D.M. Tailoring optical properties of surfaces in wide spectral ranges by multi-scale femtosecond-laser texturing: A case-study for TaB₂ ceramics. *Opt. Mater.* **2020**, *109*, 110347. [[CrossRef](#)]
19. Sciti, D.; Trucchi, D.; Bellucci, A.; Orlando, S.; Zoli, L.; Sani, E. Effect of surface texturing by femtosecond laser on tantalum carbide ceramics for solar receiver applications. *Sol. Energy Mater. Sol. Cells* **2017**, *161*, 110347. [[CrossRef](#)]
20. Serpente, V.; Bellucci, A.; Girolami, M.; Mastellone, M.; Mezzi, A.; Kaciulis, S.; Carducci, R.; Polini, R.; Valentini, V.; Trucchi, D. Ultra-thin films of barium fluoride with low work function for thermionic-thermophotovoltaic applications. *Mater. Chem. Phys.* **2020**, *249*, 122989. [[CrossRef](#)]
21. Shih, A.; Yater, J.; Hor, C. Ba and BaO on W and on Sc₂O₃ coated W. *Appl. Surf. Sci.* **2005**, *242*, 35–54. [[CrossRef](#)]
22. Jin, F.; Beaver, A. Barium strontium oxide functionalized carbon nanotubes thin film thermionic emitter with superior thermionic emission capability. *J. Vac. Sci. Technol. B* **2017**, *35*, 41202. [[CrossRef](#)]
23. Sharma, A.; Shukla, S.; Rai, K. Finite time thermodynamic analysis and optimization of solar-dish Stirling heat engine with regenerative losses. *Therm. Sci.* **2011**, *15*, 995–1009. [[CrossRef](#)]
24. Renewable Energy Agency International IRENA. *Renewable Energy Market Analysis: GCC 2019*; Renewable Energy Agency International IRENA: Masdar City, Abu Dhabi, 2019.
25. El Hamdani, F.; Vaudreuil, S.; Abderafi, S.; Bounahmidi, T. Determination of design parameters to minimize LCOE, for a 1 MWe CSP plant in different sites. *Renew. Energy* **2021**, *169*, 1013–1025. [[CrossRef](#)]
26. Dersch, J.; Dieckmann, S.; Hennecke, K.; Pitz-Paal, R.; Taylor, M.; Ralon, P. LCOE reduction potential of parabolic trough and solar tower technology in G20 countries until 2030. *AIP Conf. Proc.* **2020**, *2303*, 120002. [[CrossRef](#)]
27. Christoph Kost, Fraunhofer ISE, Study: Levelized Cost of Electricity- Renewable Energy Technologies. June 2021. Available online: <https://www.ise.fraunhofer.de/en/publications/studies/cost-of-electricity.html> (accessed on 29 December 2022).
28. Zhao, L.-D.; Lo, S.-H.; Zhang, Y.; Sun, H.; Tan, G.; Uher, C.; Wolverton, C.; Dravid, V.P.; Kanatzidis, M.G. Ultralow thermal conductivity and high thermoelectric figure of merit in SnSe crystals. *Nature* **2014**, *508*, 373–377. [[CrossRef](#)] [[PubMed](#)]
29. Bellucci, A.; Mastellone, M.; Girolami, M.; Orlando, S.; Medici, L.; Mezzi, A.; Kaciulis, S.; Polini, R.; Trucchi, D.M. ZnSb-based thin films prepared by Ns-PLD for thermoelectric applications. *Appl. Surf. Sci.* **2017**, *418*, 589–593. [[CrossRef](#)]
30. Cappelli, E.; Bellucci, A.; Medici, L.; Mezzi, A.; Kaciulis, S.; Fumagalli, F.; Di Fonzo, F.; Trucchi, D. Nano-crystalline Ag–PbTe thermoelectric thin films by a multi-target PLD system. *Appl. Surf. Sci.* **2015**, *336*, 283–289. [[CrossRef](#)]
31. Santagata, A.; Pace, M.L.; Bellucci, A.; Mastellone, M.; Bolli, E.; Valentini, V.; Orlando, S.; Sani, E.; Failla, S.; Sciti, D.; et al. Enhanced and Selective Absorption of Molybdenum Nanostructured Surfaces for Concentrated Solar Energy Applications. *Materials* **2022**, *15*, 8333. [[CrossRef](#)]
32. Hernández-Moro, J.; Martínez-Duart, J. Analytical model for solar PV and CSP electricity costs: Present LCOE values and their future evolution. *Renew. Sustain. Energy Rev.* **2013**, *20*, 119–132. [[CrossRef](#)]

Disclaimer/Publisher’s Note: The statements, opinions and data contained in all publications are solely those of the individual author(s) and contributor(s) and not of MDPI and/or the editor(s). MDPI and/or the editor(s) disclaim responsibility for any injury to people or property resulting from any ideas, methods, instructions or products referred to in the content.